STATISTICAL STUDIES OF THE RELATIONSHIP BETWEEN THE AMPLITUDE OF POSITIVE MAGNETIC BAYS AT MID LATITUDES, GEOMAGNETIC ACTIVITY AND SOLAR WIND PARAMETERS

A. A. Lubchich[a], *, I. V. Despirak[a], **, R. Werner[b], ***

[a]*Polar Geophysical Institute, Apatity, Russia*

[b]*Space Research and Technology Institute, Bulgarian Academy of Sciences, Stara Zagora, Bulgaria*

**e-mail: lubchich@pgia.ru*

***e-mail: despirak@gmail.com*

****e-mail: rolwer52@yahoo.co.uk*

Received March 03, 2024

Revised June 23, 2024

Accepted July 25, 2024

Abstract. During the expansion phase of the substorm, the poleward jump of the aurora (breakup) and the expansion of the auroral bulge are observed. The expansion is accompanied by a negative magnetic bay under the aurora and a positive magnetic bay at the middle latitudes. The amplitude of the negative bay is characterized by the auroral AL index. To characterize the positive bay, the MPB index (Mid-latitude Positive Bay index) was previously proposed. The paper examines the statistical relationship of the MPB index with the geomagnetic activity at different latitudes and with the parameters of the solar wind and the interplanetary magnetic field. It is shown that all extremely large values of the MPB index (above 10,000 nT^2) are observed during strong geomagnetic storms (when the Dst index drops below –100 nT), and all extremely strong geomagnetic storms (when the Dst index drops below –250 nT) accompanied by extremely high MPB index values. Statistically, the MPB index increases with the increasing of geomagnetic activity at any latitudes. The MPB index, on average, increases with the increasing of the magnitude of the interplanetary magnetic field and any of its components. But for the Bz component, large values of the MPB index are observed by its southward direction. For plasma parameters of the solar wind, the MPB index increases most strongly with the increasing of the solar wind speed. There is also the strong dependence on the dynamic pressure and on the magnitude of the E_Y component of the solar wind electric field. However, the MPB index weakly depends on solar wind density and temperature.

Keywords: *geomagnetic indices, magnetic storms, solar wind, interplanetary magnetic field, statistical analysis*

DOI: 10.31857/S00167940250605e7

1. INTRODUCTION

The jump of auroras toward the pole (breakup) and the expansion of the auroral bulge are important signs of a magnetospheric substorm. The expansion of the auroral bulge is accompanied by the development of negative magnetic bays at auroral latitudes and positive magnetic bays at mid-latitudes. The appearance of magnetic bays is caused by the development of the current wedge of the substorm arising due to partial destruction of the transverse (morning- evening) current of the near-tail of the magnetosphere, for example, due to reconnection of the geomagnetic field lines. As a result, a large-scale three-dimensional current system is formed in which a section of the destroyed current of the magnetospheric tail is redirected along the geomagnetic field lines to the ionosphere, is short-circuited in the auroral latitudes by the western electrojet and returns to the magnetosphere in the evening sector in the form of a longitudinal current created by the precipitating accelerated electrons. Very intense substorms, during which the *SML*-index of geomagnetic activity falls below -2500 nTL, are often distinguished into a separate class - superstorms [Tsurutani et al., 2015; Hajra et al., 2016 and others]. During supersubstorms, an additional current wedge of opposite direction on the evening side can form (e.g., [Fu et al., 2021; Zong et al., 2021; Despirac et al., 2022]).

The mid-latitude positive magnetic cove in the *X*-component of the magnetic field at stations in the near-midnight sector, associated with the development of the current wedge of the substorm, consists of a short, lasting on the order of 20 min, growth phase and a generally slightly slower decline phase. At a fixed point in time, the spatial distribution of positive variations in the *X* component is a Gaussian-shaped profile symmetric about the center of the current wedge. The spatial variation in the *Y-component* resembles one cycle of a sine wave with a maximum in the evening sector, at the longitude of the outgoing current, and a minimum in the morning sector, at the longitude of the incoming current (details are shown, for example, in Fig. 9 of McPherron et al. [1973]). Thus, the position of the extrema of the northern and eastern components of the magnetic field can be used to characterize the substorm current wedge.

Using this circumstance, a new one-minute geomagnetic *MPB* index (*Mid-latitude Positive Bay index*) was recently introduced in 2015 to analyze the manifestations of substorm activity at *mid-latitudes*. The methodology of its calculation is described in detail in [Chu, 2015; McPherron and Chu, 2017, 2018]. The index characterizes the power of perturbations of the horizontal component of the magnetic field at mid-latitude stations during the development of the current wedge of a substorm. It is determined by the sum of the squares of perturbations of the northern and eastern components of the magnetic field.

The authors of the index (McPherron and Chu) proposed two different in details calculation methods, which led to the creation of two similar, but still slightly different, sets of MPB-index values. A description of the differences in the calculation methodologies can be found, for example, in McPherron and Chu [2017]. One difference is that the first set (let us call it the McPherron list) is derived from data from 35 stations with geomagnetic latitude λ_{mag} between -45° and 45° , whereas the second set (the Chu list) is derived from data from 41 stations in the Northern and Southern Hemispheres with $20° < |\lambda_{mag}| < 52°$. The first list can be found in the supplementary information to the online version of the paper by McPherron and Chu [2018]. It includes one-minute values of the total power of the total horizontal magnetic field variations, i.e. $\Delta X^2+\Delta Y^2$, for the period from February 1980 to the end of 2012 (until the end of 1984, the data are episodic, irregular). The Chu list, at the time of its presentation, included separately the one-minute variations ΔX^2 (we will denote them as *MPB-X*), ΔY^2 (*MPB-Y*), and their sum from the beginning of 1991 to the end of 2019. It will be used in our work. Therefore, let us briefly describe the algorithm for obtaining the *MPB*-index according to Chu's method. First, the secular variations and solar-diurnal *Sq* variations are removed from the initial data of magnetic field measurements at the 41st station. The former are removed using a linear trend, the latter - using the 21-day epoch superposition method. Then, the remaining low-frequency variations are removed using an upper-pass filter with a cutoff frequency at 12 hours. Next, only data from stations currently in the night sector ±5 h from 23.5 h local time are retained. These data are squared and averaged over all "night" stations. As a result, *MPB-X* and *MPB-Y* values are obtained. Their sum gives the total *MPB-index* at a given time.

Sometimes it is of interest to analyze the magnetic field variations at a particular magnetic station at midlatitudes. Such a possibility is described in [Werner et al., 2021], where an improved methodology for calculating the *MPB*-index was proposed. In particular, data from the Bulgarian station Panagjurishte (Panagjurishte (PAG), 42.5° N, 24.2° E; $\lambda_{mag} \approx 37°$) were taken into account.

Note that sometimes variations of the square root of the MPB-index rather than the *MPB*-index itself are analyzed (e.g., [Sergeev et al., 2020; Tsyganenko et al., 2021]).

In this work, the *MPB*-index is statistically analyzed and its relation to both geomagnetic activity at different latitudes and solar wind (SW) and interplanetary magnetic field (IMF) parameters is investigated.

2. DATA

The one-minute *MPB*-index values for the period from 1991 to 2019 were taken for the analysis. The one-minute values of other geomagnetic indices characterizing magnetic activity at different latitudes were taken for the same period. Let us list them moving from the pole to the equator.

– To characterize the perturbation in the northern polar cap, we will use the *PC*(*N*)-index [Troshichev and Andrezen, 1985; Troshichev et al., 1988; Troshichev, 2010]. The index values are available in the OMNI database on the website (https://cdaweb.gsfc.nasa.gov/). As is known, the *PC*-index is calculated from the data of one station located near the geomagnetic pole. In the Northern Hemisphere, for the *PC*(*N*) index, this is Qaanaaq (Thule) station (Qaanaaq (Thule) (THL), 77.5° N 290.8° E; $\lambda_{mag} \approx 86.7°$); in the Southern Hemisphere, for the *PC*(*S*) index, this is Vostok station. The *PC-index* is proportional to the geoeffective interplanetary electric field and is an indicator of the amount of energy entering the Earth's magnetosphere [Troshichev and Andrezen, 1985; Troshichev et al., 1988; Troshichev, 2010].

– Perturbations in the auroral zone are characterized by the indices of the *AE* family (*AE*, *AL*, *AO*, *AU*), determined from data of 12 auroral stations. The *AL* and *AU* indices are determined by the maximum for these stations negative and positive deviation of the *H* component *of* the geomagnetic field from the quiet level and depend on the intensity of the western and eastern auroral electric jet current. The *AE*-index determines the total magnitude of deviations of the *H*-component of the geomagnetic field, i.e., it is equal to the sum of the moduli of the *AL*- and AU-indices. The *AO*-index is equal to the half-sum of the *AL*- and *AU*-indices. The indices are available on the website (https://wdc.kugi.kyoto-u.ac.jp/aeasy/index.html).

-The SML and *SMU* indices are determined similarly to the *AL* and *AU* indices, but using data from all magnetic stations of the SuperMAG project with geomagnetic latitudes from +40 to +80° . The indices are available on the website (http://supermag.jhuapl.edu/indices/). They better describe the processes in the auroral oval in strongly perturbed conditions, for example, during magnetic storms, when the auroral oval can deviate strongly toward the equator from its position in quiet conditions. At such deviations, the stations used in the calculation of indices of the *AE* family may be outside the auroral oval region; as a consequence, the *AE*-index will no longer reflect the intensity of electric jets [Feldstein, 1992].

-Indices *ASY-H*, *ASY-D* and *SYM-H*, *SYM-D* are available at (https://wdc.kugi.kyoto-u.ac.jp/aeasy/index.html). The procedure for calculating and analyzing the indices, for example, for 1992, one of the first years analyzed in this work, is described in detail in [Iyemori et al., 1994]. Data from nine geomagnetic stations located at middle and low latitudes are used, including three stations used for calculating the *Dst*-index. Monthly indices are calculated for six stations out of the nine; the choice of the six stations may be different in different months. *SYM-H* is essentially the average deviation of the *H* component of the geomagnetic field from the quiet level at the selected stations, corrected for their geomagnetic latitudes, similar to the procedure for calculating the *Dst*-index. *SYM-D* is calculated from the averaged deviations of the *D*-component of the geomagnetic field, but without correction for the latitudes of the stations. The *SYM-H* and *SYM-D* indices characterize the longitudinally symmetric part of the ring current. The indices *ASY-H* and *ASY-D* determine the range between the maximum and minimum values of the *H*- and *D*-components of the geomagnetic field at six stations after subtracting the corresponding symmetric parts from the perturbation field and thus characterize the longitudinally asymmetric part of the ring current. We will refer *ASY-H* and *ASY-D* to the midlatitude indices, since their calculation uses data from midlatitude stations as well. Wanliss and Showalter [2006] concluded that, as a rule, the *SYM-H* index does not differ much from the low-latitude *Dst* index, and it can be used as a *Dst* index with high (one-minute) resolution. On this basis, we categorize *SYM-H* and *SYM-D* as low-latitude indices.

- Average hourly values of Dst-index - from the site (https://wdc.kugi.kyoto-u.ac.jp/dst_final/index.html).

One-minute values of the MMP modulus B_T and its components *Bx*, *By*, *Bz* (in *GSE* and *GSM* systems) and NE data (velocity magnitude and its components, density, temperature, dynamic pressure, as well as E_Y-component of the electric field and the ratio of plasma pressure to magnetic pressureβ) are taken from the OMNI database from the site (https://cdaweb.gsfc.nasa.gov/).

3. RESULTS

3.1 Cases of observing extremely large MPB-index values

Most of the *MPB*-index increases are associated with substorm activity. The criterion for determining the moment of substorm by *MPB*-index variations is when the peak value of *MPB*-index exceeds 25 nTL^2 [McPherron and Chu, 2017, 2018]. But sometimes the MPB-index reaches very large values. We selected all cases of *MPB-X* exceeding 10,000 nTL^2 (i.e., when the variation of Δ*X* exceeded 100 nTL).

Fig. 1.

An example of such an event is presented in Fig. 1, which shows the values of the modulus and two components of the *MPB*, several CB values and geomagnetic indices for 24 h beginning from 12:00 UT 06.04.2000. It can be seen that the *MPB*-index exceeds 10 000 nTl^2 (this value is shown in the plot by the dashed line), reaching ~60 000 nTl^2 during the main phase of the magnetic storm c Dst_{min} = –288 nTl. Often magnetic storms are divided into groups according to the value of Dst_{min}. Storms with Dst_{min} < –100 nTl are considered to be strong (*intense*) magnetic storms [e.g., Gonzalez and Tsurutani, 1987]. Tsurutani et al. [1992] considered five very intense (*great*) magnetic storms with Dst_{min} of –249 nTL and below. Mac-Mahon and Gonzalez [1997] called such very intense magnetic storms superstorms, using the criterion Dst_{min} < –240 nTl. Later, in [Gonzalez et al., 1999, 2002], the numerical criterion for very intense magnetic storms was refined: Dst_{min} < –250 nTl. We will use this refined criterion in the following. According to this criterion, the extremely high values of the *MPB*-index shown in Fig. 1 were observed during the superstorm. It can be seen from Fig. 1

that the differences between the *SYM-H* and *Dst* indices, if their different time resolution is not taken into account, are insignificant, which justifies categorizing *SYM-H* as a low-latitude index. It can also be seen that during the main phase of the storm, the difference between the *SML* and *AL* indices can indeed be significant; the indices can differ in magnitude by a factor of two or more.

Superstorms are a rare phenomenon, with only 39 events recorded between 1957 and 2018, a list of which is given in [Meng et al., 2019], of which only 14 have been observed since 1991, when data are available for *MPB*-index values in the Chu list we use. The analysis shows that there were observations of extremely large *MPB*-index values during all 14 events. This can be seen from Table 1, in which the superstorms recorded since 1991 are ranked by the magnitude of the minimum *Dst*-index value. The first five columns are taken from Table 1 in Meng et al. [2019]. The last column summarizes the magnitude and time of registration of the extreme value of *MPB*-index.

Table 1.

Note that during two storms - 08.11.2004 and 06.11.2001 - *MPB-X* was below the specified threshold value, nevertheless the full *MPB*-index exceeded 10 000 nTL^2.

As a rule, the maximum values of the *MPB*-index were registered not far from the moment of the *Dst* minimum, the average time difference between these events was ~3 hours. But in the last two superstorms (10.11.2004 and 29.10.1991), the moment of the maximum of the *MPB*-index was closer to the moment of observation of the sudden SI^+ pulse.

The remaining events with extremely large *MPB-index* values (*MPB-X* > 10 000 nTL^2) were during strong magnetic storms (Dst_{min} < –100 nTL). The corresponding results are summarized in Table 2. Since the *Dst*-index has an hourly resolution, the time in the second column turns out to be a multiple of 30 min - the middle of an hour or, for the storm of 06.02.1992, the middle of a two-hour interval with the minimum *Dst*-index value. The first storm in the table with Dst_{min} = –247 nTL is sometimes also referred to superstorms (e.g., [Gonzalez et al., 2011]). In most cases, the extreme values of the *MRW index* were observed near the time of registration of the minimum *SYM-H* index value.

Table 2.

Note that nine more superstorms were recorded between 1980 and 1990, when *MPB*-index data from the first list are available [McPherron and Chu, 2018]. Anomalously high *MPB*-index values (> 10,000 nTL^2) were also recorded during all these superstorms.

3.2 Statistical relationship between MPB-index and geomagnetic indices

All one-minute *MPB-index* data for the entire analyzed interval from 1991 to 2019 were taken, with no additional analysis of whether the observed variations were accompanied by the development of substorms or not.

Fig. 2.

The distribution of *MPB-index* by values is shown in Fig. 2. The tail of the distribution in double logarithmic scale is well approximated by a straight line with negative slope ~ –2.3 (wide gray line on the graph), i.e., it has a steppe form: $N \approx b \times MPB^{-2.3}$. The graph is plotted in steps of *MPB*-index values of 1 nTl^2, including well describing the region of small index values, up to the substorm threshold value of 25 nTl^2. A graph with a step of 100 nTl^2 describing the region above the threshold value is given in [Lubčić et al., 2023]. It is well described by a power law in the whole region of values with a close exponent of degree: –2.5.

Such a stepped distribution can be considered as a special case of the Pareto distribution (e.g., [Arnold, 2015]). Steppe distributions fall slower than exponential distributions, due to which they are often used to analyze the distribution of extreme values. For example, [Tsubouchi and Omura, 2007] used the Pareto distribution to analyze the probability of strong magnetic storms. They showed that the intensity distribution of storms becomes stepped at *Dst* < –280 nTL. This threshold value is close to the criterion of superstorms, which confirms the statistical validity of the introduction of this separate class of storms. [Nakamura et al., 2015] analyzed the distribution of *AL*-, *AU*-, and *AE* -indices using a Pareto distribution and concluded that there should be limit values of the indices: *AL* ~ –4200 nTL and *AU* ~ 2000 nTL, i.e., the current should have a limit value in the western and eastern electrojet. They analyzed the period from 1996 to 2012. Our work considers the interval 1991− 2019. The lowest AL-index value for our interval turned out to be equal to –4141 nTl and occurred during the main phase of the most powerful magnetic storm (20.11.2003, Dst_{min} = –422 nTl).

An example of another type of distributions used, among others, in extreme value theory is the Weibull distribution [Weibull, 1951; Coles, 2001]. Werner et al. [2023] showed that the distribution of the number of positive bay events at mid-latitudes as a function of the local AL-index determined from selected stations of the IMAGE (*International Monitor for Auroral Geomagnetic Effects*) magnetometer network (*IL*-index -IMAGE *electrojet Lower index*) are well described by the Weibull distribution. In particular, the recurrence of events with given extreme values of the *IL-index* was evaluated.

We analyzed the statistical relationship of the *MPB*-index with other one-minute geomagnetic indices. For this purpose, we constructed regression lines of the *MPB*-index with respect to the indices mentioned in Section 2. The dependence of any value of *Y* on the value of *X* is manifested in the change of the average values of *Y* when *X* changes. To determine this dependence, the *X* array was divided into uniform segments X_i, and at each segment the average value of Y_i was calculated. The dependence of *X* on *Y* can be determined in a similar way. As we know, if there is no direct functional relationship, the dependencies *Y*(*X*) and *X*(*Y*) will not coincide.

Fig. 3.

The relationship between the *MPB* index and the *SML* index is shown by Fig. 3. Fig. 3*a* shows the distribution of the *SML* index by values. Similar to Fig. 2, the graph is plotted in double logarithmic scale, so the *SML* module was taken. The tail of the distribution in double logarithmic scale is approximated by a straight line with slope ~ –5.2 (wide gray band in the graph). As can be seen from Fig. 3*b*, the *MPB* index increases monotonically with increasing auroral activity, the indicator of which is the *SML* index. The dependence of *MPB* on *SML* is close to a steppe - the approximation is shown in Fig. 3*b* for *SML* values < –300 nTL, degree exponent ~2.3. The inverse dependence shown in Fig. 3*c*, has a different form: *SML* -index at first decreases (grows modulo) with *MPB* growth, then, at reaching *MPB* ~ 4000 nTl^2, comes to the horizontal asymptote equal to about –1100 nTl (horizontal segment on the graph).

Fig. 4.

Fig. 4 shows the statistical dependence of the *MPB*-index on the geomagnetic indices characterizing perturbations in the polar cap (Fig. 4*a*, *PC*(*N*)-index), at middle (Fig. 4*b*, *ASY-H* index) and low (Fig. 4*c*, *SYM-H* index) latitudes. The *MPB*-index is more strongly dependent on positive values of the *PC*(*N*)-index, monotonically increasing with their increase. At *PC*(*N*) > 2, the increase is close to a stepwise increase with a degree exponent slightly higher than two (2.35) (shown by the gray bar on the right part of Fig. 4*a*). As is known, a positive *PC*(*N*)-index characterizes the impact of the geoeffective interplanetary electric field; substorms and magnetic storms begin when the *PC*-index exceeds a threshold value of ~2 mV/m [Troshichev, 2010]. And negative values of the PC-index are connected with the impact of the northern component of the IMF on the magnetosphere. In this region, the growth of the MPB-index is close to exponential (the gray broad line in the left part of Fig. 4*a*, for *PC*(*N*) < 0. The *MPB*-index monotonically grows with the growth of the *ASY-H* index; at *ASY-H* > 20 nTl, the dependence is steppe (shown by the gray line in Fig. 4*b*), and the degree exponent is the same as at *PC*(*N*) > 2. The *MPB*-index monotonically grows with the growth of the modulus of the *SYM-H* index, depending more strongly on its negative values. At *SYM-H* < –50 nTl the growth is stepwise, quadratic, i.e. $|SYM-H|\sim\sqrt{MPB}$. At positive values, the growth of *MPB*-index is close to exponential. Both dependencies are shown by gray lines in Fig. 4*c*.

3.3 Correlation of the MPB-index with the parameters of the solar wind and the interplanetary magnetic field

For the analysis we will use minute data from the OMNI database: the magnitude of the MMP and the magnitude of its components in two Cartesian coordinate systems - *GSE* and *GSM*, the magnitude and direction of the NE velocity, its density, temperature, and dynamic pressure, as well as the geoeffective component of the electric field and the parameter β , equal to the ratio of the plasma thermal pressure to the magnetic pressure.

Fig. 5.

The dependence of the *MPB*-index on the characteristics of the interplanetary magnetic field is shown in Fig. 5. As can be seen from Fig. 5*a*, the *MPB*-index grows monotonically with the growth of the MMP modulus B_T, approaching the extreme values at very large values of B_T. The regression line on the By-component of the MMP depends weakly on the sign of the component, i.e., the graph is almost symmetric with respect to the zero value of *By* (Fig. 5*b*). The *MPB*-index increases with increasing modulus of the *Bz*-component of the MMP (Fig. 5*c*), but it is much higher at negative values of *Bz* - for example, *MPB* is ~10 times larger at *Bz* = –30 nTl than at *Bz* = +30 nTl. Fig. 5 is plotted in the *GSM* coordinate system. The corresponding dependences for the MPB components in the *GSE* system are given in [Lubčić et al., 2023].

The plasma parameters of the solar wind that most affect the *MPB-index* are its velocity *V* (and radial component V_X), and the dynamic pressure P_{dyn}. The dependence of the MPB-index on V_X is close to exponential (the approximation is shown in Fig. 6*a* by the gray line). When the velocity changes by a factor of four, from 250 to 1000 km/s, the MPB-index varies almost from zero to ~2 000 nTl^2. The dependence of the MPB-index on the dynamical pressure of the solar wind for values of $P_{dyn} \leq 40$ nPa is close to steppe, with an exponent of degree 1.3 (gray line in Fig. 6*b*). The MPB-index varies within approximately the same range as in Fig. 6*a*). The MPB-index grows almost linearly with increasing solar wind density, but the range of index variations is relatively small - from ~30 to ~300 nTL^2, therefore the dependence of the MPB-index on the NE density can be considered weak. Because of this, at very large values of the dynamic pressure of the CB ($P_{dyn} > 40$ nPa), observed usually at high density and not very high solar wind speed, the dependence of the *MPB-index* on P_{dyn} reaches saturation (*MPB* ~ 2000 nTL^2) or even starts a small decrease of the MPB-index values at further growth of the dynamic pressure of the solar wind. However, this result is statistically unreliable due to the small number of such extreme events. At CB temperatures up to 10 000 K we have $MPB \approx 40$ nTl^2, then the *MPB* value decreases by almost a factor of two, reaching its minimum value at $T \approx 14$ 000 K, and then begins to increase monotonically, almost linearly, reaching 700 nTl^2at a temperature of one million degrees Kelvin. The MPB-index strongly depends on the geoeffective component of the solar wind electric field ($E_{Y\,GSM}$). The dependence of the MPB-index on $E_{Y\,GSM}$ (Fig. 6*c*) is similar to that of the *PC*(*N*)-index (Fig. 4*a*). By analogy with Fig. 4*a* in the left part of Fig. 6*c*, for $E_{Y\,GSM}$ from -15 mV/m to 0, shows an exponential approximation, while the right side, for $E_{Y\,GSM}$ from 2 to 30 mV/m, shows a stepwise approximation. The MPB-index is almost independent of the magnitude of the plasma β.

Fig. 6.

4. DISCUSSION

In Section *3.1*, it was shown that all cases of observations of extremely large values of the *MPB*-index were during the development of strong (–250 nTl < Dst_{min} ≤ –100 nTl) and very strong (Dst_{min} ≤ –250 nTl) magnetic storms (superstorms). During magnetic storms there is an expansion and displacement of the auroral oval towards the equator. At this time, the middle latitudes, where the magnetic stations used to calculate the *MRV* index are located, become auroral or close to it, which explains the detected dependence.

During the two strong magnetic storms shown in Table 2 (01.10.2002 and 26.02.1992), even the minimum one-minute values of the *SYM-H* index turned out to be greater than the average hourly value Dst_{min}. One can assume that this is due to differences in the list of the stations used, in the methodology of determining the baselines and so on. Comparison of *Dst* and *SYM-H* indices is carried out, for example, in [Wanliss and Showalter, 2006].

The correlation relation of the *MPB*-index, introduced in Section *3.2.* to analyze the manifestations of substorm activity at middle latitudes, with the increasing deviation from the quiet level of other geomagnetic indices can be explained as follows. The size of the polar aurora oval depends on the magnetic activity. Under quiescent conditions, it resembles a ring with a width of ~2°. With increasing magnetic activity, the size of the oval increases, and this is most significantly observed on the night side, where the expansion goes both toward the pole and the equator. At large perturbations, the width of the oval can exceed 10° [Starkov, 2000], which may have an impact on magnetic measurements at different latitudes. The regression lines of the *PC*(*N*), AL,$\sqrt{MPB}$, *ASY-H*, and *SYM-H* indices with respect to the SML index were determined. The dependencies obtained were found to be close to linear. For the root of *MPB* we have: $\sqrt{MPB} \approx -0.029 \times SML - 1.09$, for the other indices the corresponding expressions are given in [Lubčić et al., 2023]. The correlation coefficient R between $\sqrt{MPB}$ and SML is –0.79. Note that the modulus of the correlation coefficient is maximal between AL and SML indices (R ≈ 0.95), and minimal between *SYM-H* and SML indices R ≈ 0.60. The closer the modulus of the correlation coefficient is to one, the closer the dependence is to linear. The above obtained steppe, almost quadratic, approximation dependence of the *MPB* index on the indices *PC*(*N*) > 2 (degree ~2.4), SML (2.3), *ASY-H* (2.3) and *SYM-H* (2.0) is consistent with this result, the closeness of the dependence to linear. The difference in the dynamics of the *ASY-H* and *SYM-H* indices during magnetic storms is discussed in [Dremukhina et al., 2020].

Extremely large values of the interplanetary magnetic field are usually associated with large-scale geoeffective solar wind structures, such as magnetic clouds or, as in the example in Fig. 1, the propagation of a coronal mass ejection through the unperturbed solar wind. The impact of such structures on the Earth's magnetosphere can cause the development of geomagnetic storms, which in turn can cause very large values of the *MPB*-index (see Section 3.1).

The weaker (steppe) dependence of the *MPB*-index on the dynamic pressure of the solar wind (Fig. 6*b*) compared to the exponential dependence on its velocity (Fig. 6*a*), despite the proportionality of the dynamic pressure to the square of the NE velocity, can be explained by the fact that statistically the value of the dynamic pressure of the solar wind grows weakly with the increase of its velocity. When the solar wind velocity is high, it tends to have a low density. For the period of the minimum of the 11-year solar activity cycle, a weak dependence of the dynamic pressure on the solar wind speed was shown, for example, in Lubčić et al. [2004].

5. CONCLUSIONS

The relationship of the mid-latitude *MPB* (*Mid-latitude Positive Bays*) index with geomagnetic activity and solar wind parameters has been analyzed. The following results were obtained:

- All extremely large *MPB-index* values are observed during strong and very strong (Dst_{min} < –100 nTL) geomagnetic storms. All extremely strong (Dst_{min} < –250 nTL) geomagnetic storms (superstorms) are accompanied by extremely high *MPB-index* values.

- The MPB-index statistically increases with increasing geomagnetic activity at any latitude, since there is a correlation between the geomagnetic activity at different latitudes.

- The MPB-index statistically increases with the growth of both the magnitude of the interplanetary magnetic field and the modulus of any of its components. For the *Bz*-component of the IMF, the dependence on its southern component is stronger.

- The dependence of the MPB-index on the solar wind speed is stronger. The dependence on the dynamic pressure and on the magnitude of the geoeffective component of the NE electric field is also strong. The dependence of MPB-index on solar wind density and temperature is weak.

ACKNOWLEDGEMENTS

The authors are grateful to the creators of the IMAGE (http://space.fmi.fi/image/), SuperMAG (http://supermag.jhuapl.edu/)*, and* INTERMAGNET (https://intermagnet.github.io/) databases for allowing us to use them in this work. We are grateful to the teams that created and maintain the World Data Center for Geomagnetism, Kyoto (https://wdc.kugi.kyoto-u.ac.jp/) and OMNI (https://cdaweb.gsfc.nasa.gov/) databases and provide free access to the data. We also thank for the opportunity to use the *SMU* and *SML* indices [Newell and Gjerloev, 2011]; and the collaboration with SuperMAG [Gjerloev et al., 2012].

The authors thank Xiangning Chu for kindly allowing us to use the *MPB* index values.

FUNDING

The work of Daspirak Irina Vadimovna and Ljubčić Andris Alekseević was carried out within the framework of the State Assignment of the PIP on the topic "Dynamic processes in the system "solar wind - magnetosphere - ionosphere" and their influence on the high-latitude ionosphere" (FMES-2022-002).

REFERENCES

1. *Werner R., Guineva V., Despirak I.V., Lubchich A.A., Setsko P.V., Atanassov A., Bojilova R., Raykova L., Valev D.* Statistical Studies of Auroral Activity and Perturbations of the Geomagnetic Field at Middle Latitudes // Geomagnetism and Aeronomy. V. 63. N4. P. 473–485. 2023. https://doi.org/10.1134/S0016793223600303

2. *Dremukhina L.A., Yermolaev Y.I., Lodkina I.G.* Differences in the dynamics of the asymmetrical part of the magnetic disturbance during the periods of magnetic storms induced by different interplanetary sources // Geomagnetism and Aeronomy. V. 60. N6. P. 714–726. 2020. https://doi.org/10.1134/S0016793220060031

3. *Despirak I.V., Kleimenova N.G., Lyubchich A.A., Setsko P.V., Gromova L.I., Werner R.* Global Development of the Supersubstorm of May 28, 2011 // Geomagnetism and Aeronomy. V. 62. №. 3. P. 199–208. 2022. https://doi.org/10.1134/S0016793222030069

4. *Lyubchich A.A., Despirak I.V., Werner R.* Dependence of the MPB index on geomagnetic activity and solar wind characteristics // Proc. XLVI Annual Seminar. Apatity. P. 42–47. 2023. https://doi.org/10.51981/2588-0039.2023.46.009

5. *Lyubchich A.A., Despirak I.V., Yakhnin A.G.* Correlation between the solar wind pressure and velocity at a minimum of the 11-year cycle // Geomagnetism and Aeronomy. V. 44. No. 2. P. 143–148. 2004.

6. *Starkov G.V.* Planetary dynamics of auroral glow / Physics of near-Earth space. Chapter 3, 4. P. 409–499. Apatity: pub. KSC RAS, 706 p. 2000.

7. *Troshichev O.A.* PC-index – a ground-based indicator of solar wind energy entering the magnetosphere // Problems of the Arctic and Antarctic. No. 2 (85). P. 102–116. 2010.

8. *Arnold B.C.* Pareto Distribution / In Wiley StatsRef: Statistics Reference Online (eds N. Balakrishnan, T. Colton, B. Everitt, W. Piegorsch, F. Ruggeri and J.L. Teugels). 2015. https://doi.org/10.1002/9781118445112.stat01100.pub2

9. *Chu X.* Configuration and generation of substorm current wedge. Los Angeles: University of California, Los Angeles, 2015. (A dissertation submitted in partial satisfaction of the requirements for the degree Doctor of Philosophy in Geophysics and Space Physics).

10. *Coles S.* An Introduction to Statistical Modeling of Extreme Values / Springer, London. 2001.

11. *Feldstein Y.I.* Modelling of the magnetic field of magnetospheric ring current as a function of interplanetary medium parameters // Space Sci. Rev. V. 59. P. 83–165. 1992. https://doi.org/10.1007/BF01262538

12. *Fu H., Yue C., Zong Q.-G., Zhou X.-Z., Fu S.* Statistical characteristics of substorms with different intensity // J. Geophys. Res.: Space Physics. V. 126. e2021JA029318. 2021. https://doi.org/10.1029/2021JA029318

13. *Gonzalez W.D., Echer E., Tsurutani B.T., de Gonzalez A.L.C., Dal Lago A.* Interplanetary origin of intense, superintense and extreme geomagnetic storms // Space Science Reviews. V. 158. N 1. P. 69–89. 2011. https://doi.org/10.1007/s11214-010-9715-2

14. *Gonzalez W.D., Tsurutani B.T.* Criteria of interplanetary parameters causing intense magnetic storms (Dst < −100 nT) // Planetary and Space Science. V. 35. N 9. P. 1101–1109. 1987. https://doi.org/10.1016/0032-0633(87)90015-8

15. *Gonzalez W.D., Tsurutani B.T., Clúa de Gonzalez A.L.* Interplanetary origin of geomagnetic storms // Space Sci. Rev. V. 88. N 3-4. P. 529–562. 1999. https://doi.org/10.1023/A:1005160129098

16. *Gonzalez W.D., Tsurutani B.T., Lepping R.P., Schwenn R.* Interplanetary phenomena associated with very intense geomagnetic storms // Journal of Atmospheric and Solar-Terrestrial Physics. V. 64. N 2. P. 173–181. 2002. https://doi.org/10.1016/S1364-6826(01)00082-7

17. *Hajra R., Tsurutani B.T., Echer E., Gonzalez W.D., Gierloev J.W.* Supersubstorms (SML < −2500 nT): Magnetic storm and solar cycle dependences // J. Geophys. Res. V. 121. P. 7805–7816. 2016. https://doi.org/10.1002/2015JA021835

18. *Iyemori T., Araki T., Kamei T., Takeda M.* Mid-latitude Geomagnetic Indices “ASY” and “SYM” (Provisional). N3. 1992 // Data Analysis Center for Geomagnetism and Space Magnetism Faculty of Science Kyoto University, ISSN 0918-5763, 1994.

19. *Mac-Mahon R.M., Gonzalez W.D.* Energetics during the main phase of geomagnetic superstorms // J. Geophys. Res. V. 102. A7. P. 14199–14207. 1997. https://doi.org/10.1029/97JA01151

20. *McPherron L.R., Chu X.* The Mid-Latitude Positive Bay and the MPB Index of Substorm Activity // Space Sci. Rev. V. 206. P. 91–122. 2017. https://doi.org/10.1007/s11214-016-0316-6

21. *McPherron L.R., Chu X.* The midlatitude positive bay index and the statistics of substorm occurrence // J. Geophys. Res.: Space Physics. V. 123. N 4. P. 2831–2850. 2018. https://doi.org/10.1002/2017JA024766

22. *McPherron R.L., Russell C.T., Aubry M.P.* Satellite studies of magnetospheric substorms on August 15, 1968: 9. Phenomenological model for substorms // J. Geophys. Res. V. 78. N 16. P. 3131–3149. 1973. https://doi.org/10.1029/JA078i016p03131

23. *Meng X., Tsurutani B.T., Mannucci A.J.* The Solar and Interplanetary Causes of Superstorms (Minimum Dst ≤ −250 nT) During the Space Age // J. Geophys. Res.: Space Physics. V. 124. N 6. P. 3926–3948. 2019. https://doi.org/10.1029/2018JA026425
24. *Nakamura M., Yoneda A., Oda M., Tsubouchi K.* Statistical analysis of extreme auroral electrojet indices // Earth, Planets and Space. V. 67. Art. 153. 2015. https://doi.org/10.1186/s40623-015-0321-0
25. *Sergeev V.A., Shukhtina M.A., Stepanov N.A., Rogov D.D., Nikolaev A.V., Spanswick E., Donovan E., Raita T., Kero A.* Toward the reconstruction of substorm-related dynamical pattern of the radiowave auroral absorption // Space Weather. V. 18. N 3. e2019SW002385. 2020. https://doi.org/10.1029/2019SW002385
26. *Troshichev O.A., Andrezen V.G.* The relationship between interplanetary quantities and magnetic activity in the southern polar cap // Planet. Space Sci. V. 33. N 4. P. 415–419. 1985. https://doi.org/10.1016/0032-0633(85)90086-8
27. *Troshichev O.A., Andrezen V.G., Vennerstrøm S., Friis-Christensen E.* Magnetic activity in the polar cap – A new index // Planet. Space Sci. V. 36. N 11. P. 1095–1102. 1988. https://doi.org/10.1016/0032-0633(88)90063-3
28. *Tsurutani B.T., Gonzalez W.D., Tang F., Lee Y.T.* Great geomagnetic storms // Geophysical Research Letters. V. 19. N 1. P. 73–76. 1992. https://doi.org/10.1029/91GL02783
29. *Tsurutani B.T., Hajra R., Echer E., Gjerloev J.W.* Extremely intense (SML ≤ –2500 nT) substorms: isolated events that are externally triggered? // Annales Geophysicae. V. 33. P. 519–524. 2015. https://doi.org/10.5194/angeo-33-519-2015
30. *Tsubouchi K., Omura Y.* Long-term occurrence probabilities of intense geomagnetic storm events // Space Weather. V. 5. N 12. S12003. 2007. https://doi.org/10.1029/2007SW000329
31. *Tsyganenko N.A., Andreeva V.A., Sitnov M.I., Stephens G.K., Gjerloev J.W., Chu X., Troshichev O.A.* Reconstructing Substorms via Historical Data Mining: Is It Really Feasible? // J. Geophys. Res.: Space Physics. V. 126. N 10. e2021JA029604. 2021. https://doi.org/10.1029/2021JA029604
32. *Wanliss J.A., Showalter K.M.* High-resolution global storm index: *Dst* versus *SYM-H* // J. Geophys. Res. V. 111. N A2. A02202. 2006. https://doi.org/10.1029/2005JA011034
33. *Weibull W.* A statistical distribution function of wide applicability // J. Appl. Mech.-Trans. ASME. V. 18. N 3. P. 293–297. 1951. https://doi.org/10.1115/1.4010337
34. *Werner R., Guineva V., Atanassov A., Bojilova R., Raykova L., Valev D., Lubchich A., Despirak I.* Calculation of the horizontal power perturbations of the Earth surface magnetic field / Proceedings of the Thirteenth Workshop “Solar Influences on the Magnetosphere, Ionosphere and Atmosphere”, September, 2021, Book of Proceedings, https://doi.org/10.31401/WS.2021.proc, p. 159-165.

35. *Zong Q.-G., Yue C., Fu S.-Y.* Shock induced strong substorms and super substorms: Preconditions and associated oxygen ion dynamics // Space Sci. Rev. V. 217. N 33. 2021. https://doi.org/10.1007/s11214-021-00806-x

Table 1. List of superstorms recorded from 1991 to 2019 inclusive, ranked by the value of the minimum *Dst-index* value.

***Dst*$_{\mathbf{min}}$ time (dd.mm.yyyy UT)**	***Dst*$_{\mathbf{min}}$ (nT)**	***SYM-H*$_{\mathbf{min}}$/time (nT)/(dd.mm UT)**	***SI*$^{+}$/time (nT)/(dd.mm UT)**	**Interplanetary Case**	***MPB*/time (nT^2)/(dd.mm UT)**
20.11.2003 20:30	-422	-490/20.11 18:17	49/20.11 08:06	Sheath+MC Bxz-	~69 000/20.11 17:03
31.03.2001 08:30	-387	-437/31.03 08:06	129/31.03 01:00	Sheath+MC Bxzc-	~26 000/31.03 06:09 ~21 000/31.03 15:53
30.10.2003 22:30	-383	-432/30.10 22:55	76/30.10 20:08	Sheath	~46 000/30.10 21:35
08.11.2004 06:30	-374	-394/08.11 05:55	92/07.11 19:20	Sheath+MC Bxz-	~27 000/08.11 01:19 [MPB X~9,300]
09.11.1991 01:30	-354	-402/09.11 01:32	49/08.11 13:15	Unknown	~575 000/08.11 22:20
30.10.2003 00:30	-353	-391/30.10 01:48	81/29.10 06:14	Sheath+MC Bxz-	~69 000/29.10 19:56
16.07.2000 00:30	-301	-347/15.07 21:54	93/15.07 15:04	MC Bxz-	~23 000/15.07 21:48
25.03.1991 00:30	-298	-337/25.03 03:41	118/24.03 03:55	Unknown	~105 000/24.03 21:33 ~24 000/24.03 04:06
06.11.2001 00:30	-292	-320/06.11 04:06	88/06.11 01:54	PICME+sheath	~11 000/06.11 02:05 [MPB X~6,300]
10.05.1992 14:30	-288	-363/10.05 14:15	81/09.05 20:02	Likely sheath+MC	~28 000/10.05 18:29
07.04.2000 00:30	-288	-320/07.04 00:09	46/06.04 16:45	Sheath	~60 000/06.04 23:27
11.04.2001 23:30	-271	-280/11.04 23:57	26/11.04 15:53	Sheath	~24 000/11.04 21:37 ~23 000/12.04 00:16
10.11.2004 10:30	-263	-282/10.11 09:31	46/09.11 18:51	Sheath+MC *Bxz+*	~31 000/09.11 20:32
29.10.1991 07:30	-254	-284/29.10 08:02	51/28.10 11:03	Sheath+MC *Bxz+*	~223 000/28.10 16:06

Note: The first five columns are taken from Table 1 in Meng et al. [2019]. They are consecutively the recording time of Dst_{min} (1); its magnitude (2); the magnitude and recording time of $SYM\text{-}H_{min}$

(3); the magnitude and recording time of the sudden SI^+ pulse (4); and the structure in the solar wind that caused the magnetic storm (5). In the last column, the magnitude and time of registration of the extreme value of the *MPB*-index (6).

Table 2. Strong storms ranked by the magnitude of Dst_{min}, during which extreme *MPB*-index values were observed.

$Dst_{\min}$ time (dd.mm.yyyy UT)	$Dst_{\min}$ (nT)	$SYM\text{-}H_{\min}$/time (nT)/(dd.mm UT)	*MPB*/time (nT^2)/(dd.mm UT)
15.05.2005 08:30	-247	-305/15.05 08:20	~38 000/15.05 08:50
05.06.1991 19:30	-223	-238/05.06 16:56	~50 000/05.06 17:14
24.11.2001 16:30	-221	-234/24.11 12:37	~49 000/24.11 07:15
01.11.1991 23:30	-196	-200/01.11 19:37 20:22	~36 000/01.11 20:30
13.07.1991 15:30	-183	-238/13.07 15:42	~42 000/13.07 16:20
01.10.2002 16:30	-176	-154/01.10 12:53	~18 000/01.10 16:28
26.08.2018 06:30	-175	-206/26.08 07:11	~18 000/26.08 07:44
26.02.1992 22:00	-174	-167/26.02 22:31	~61 000/26.02 19:44
08.02.1992 16:30	-114	-126/08.02 15:18	~41 000/08.02 15:35

Note: Columns show, in sequence, the recording time of $Dst_{\min}$ (1); its magnitude (2); the magnitude and recording time of $SYM\text{-}H_{\min}$ (3); and the magnitude and recording time of the extreme value of the *MPB*-index (4).

Figure captions

Fig. 1. An example of observation of extremely large values of MPB-index during the day starting from 12:00 UT 06.04.2000. From top to bottom the behavior of the MMP modulus, *By*- and Bz-components of the MMP in the *GSM* coordinate system, velocity, density, temperature and dynamic pressure of the solar wind, as well as geomagnetic indices *PC*(*N*), *SYM-H* and *Dst*, *AL* and *SML*, *MPB* are shown.

Fig. 2. Distribution of the *MPB*-index by values plotted on a double logarithmic scale. The step on the horizontal axis is 1 nTl^2. The wide gray line shows a linear approximation of the tail of the distribution (above 200 nTl^2) in the bilogarithmic coordinate system.

Fig. 3. Distribution of -*SML*-index over values in double logarithmic scale (left), *MPB*(*SML*) (center) and *SML*(*MPB*) (right) regression lines. The gray lines show the approximation dependencies.

Fig. 4. Distribution of indices by values (top) and dependence of the *MPB* index on them (bottom). Left (*a*) for the *PC*(*N*) index, center (*b*) for the *ASY-H* index, and right (*c*) for the *SYM-H* index. The broad gray lines show the approximation dependencies.

Fig. 5. Dependence of the *MPB*-index on the MMP modulus (left) and on the *By* (center) and *Bz* (right) components of the MMP in the *GSM* coordinate system.

Fig. 6. Dependence of the MPB-index: (*a*) on the V_X-component of the NE velocity, (*b*) on the NE dynamic pressure, and (*c*) on the geoeffective electric field component $E_{Y\,GSM}$ of the solar wind. The gray lines show the approximation dependencies.

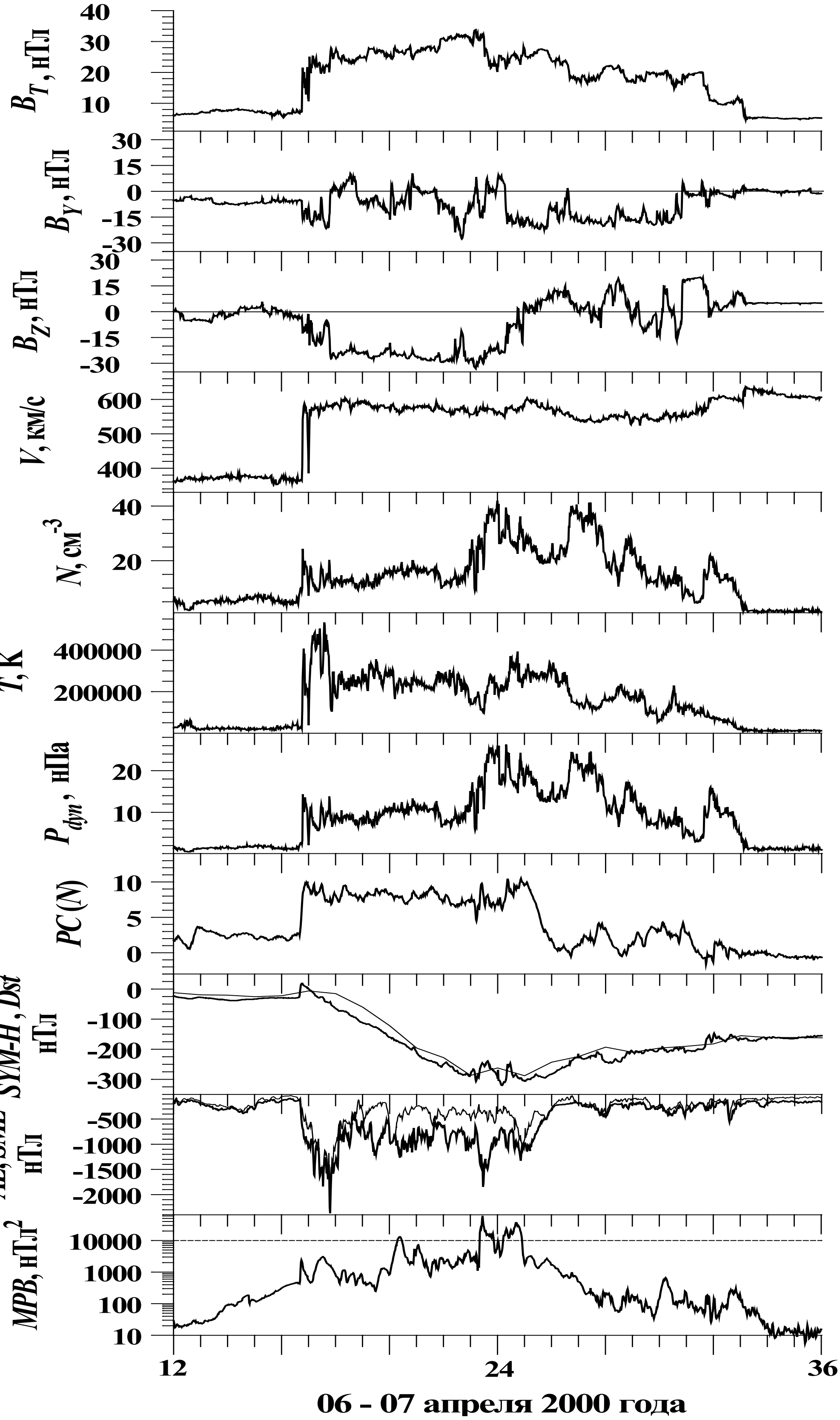

B_T, нТл
B_Y, нТл
B_Z, нТл
V, км/с
N, см$^{-3}$
T, K
P_{dyn}, нПа
$PC(N)$
$SYM\text{-}H$, Dst нТл
AL, SML нТл
MPB, нТл^2
12
24
36
06 - 07 апреля 2000 года

Fig. 1

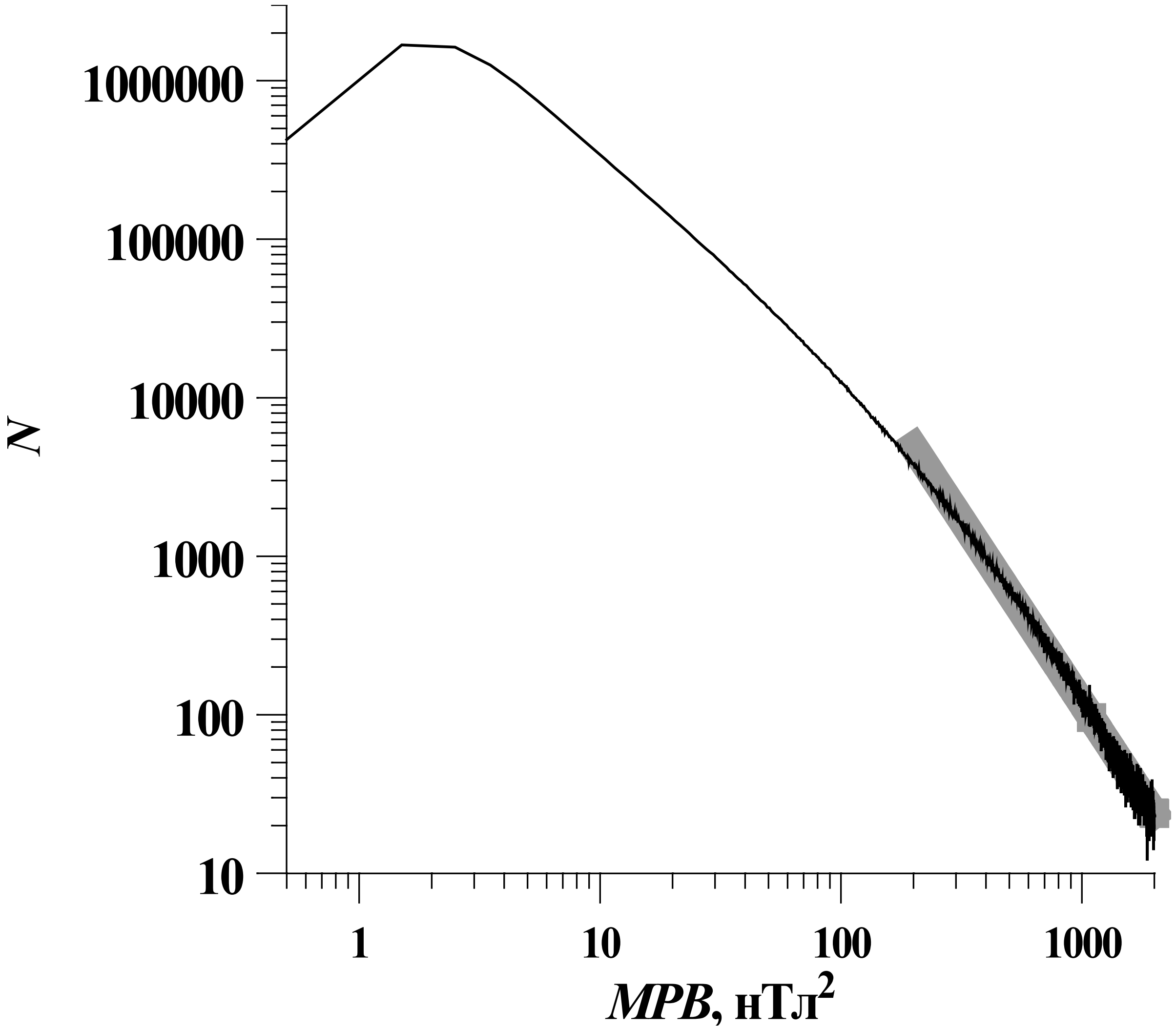

Fig. 2

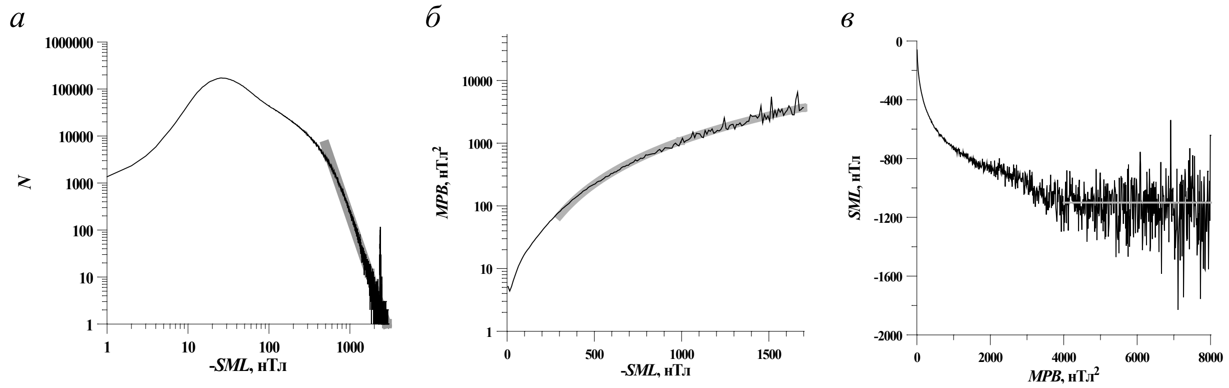

Fig. 3

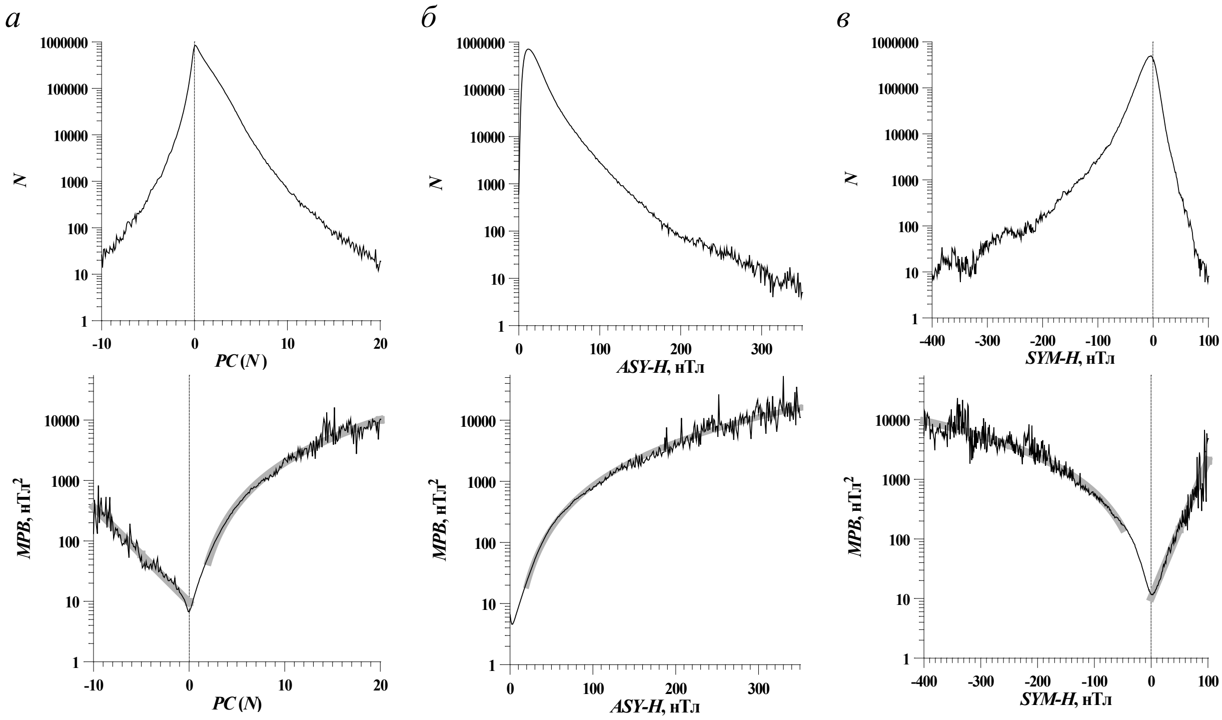

Fig. 4

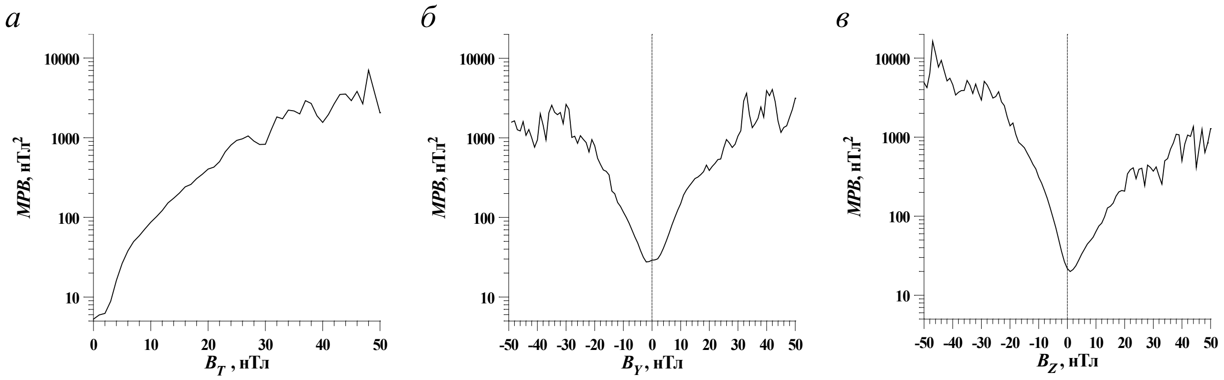
а
б
в
10000
1000
100
10
MPB, нТл2
0
10
20
30
40
50
-50
-40
-30
-20
-10
B_T , нТл
B_Y , нТл
B_Z , нТл

Fig. 5

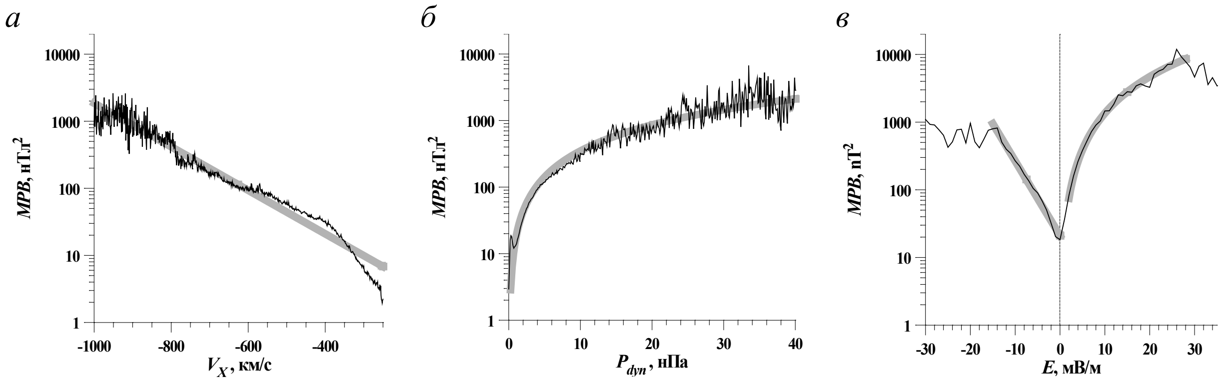

Fig. 6